Electronic, vibrational, and rotational structures in the S0 1A1 and S1 1A1 states of phenanthrene

Yasuyuki Kowaka, Takaya Yamanaka, and Masaaki Baba

Citation: J. Chem. Phys. **136**, 154301 (2012); doi: 10.1063/1.3703755
View online: http://dx.doi.org/10.1063/1.3703755
View Table of Contents: http://jcp.aip.org/resource/1/JCPSA6/v136/i15
Published by the American Institute of Physics.

Electronic, vibrational, and rotational structures in the $S_0\ ^1A_1$ and $S_1\ ^1A_1$ states of phenanthrene

Yasuyuki Kowaka,[1] Takaya Yamanaka,[2] and Masaaki Baba[1,a)]
[1]*Division of Chemistry, Graduate School of Science, Kyoto University, Kyoto 606-8502, Japan*
[2]*Instrument Center, Institute for Molecular Science, Okazaki 444-8585, Japan*

(Received 12 February 2012; accepted 29 March 2012; published online 16 April 2012)

Electronic and vibrational structures in the $S_0\ ^1A_1$ and $S_1\ ^1A_1$ states of jet-cooled phenanthrene-h_{10} and phenanthrene-d_{10} were analyzed by high-resolution spectroscopy using a tunable nanosecond pulsed laser. The normal vibrational energies and molecular structures were estimated by *ab initio* calculations with geometry optimization in order to carry out a normal-mode analysis of observed vibronic bands. The rotational structure was analyzed by ultrahigh-resolution spectroscopy using a continuous-wave single-mode laser. It has been demonstrated that the stable geometrical structure is markedly changed upon the $S_1 \leftarrow S_0$ electronic excitation. Nonradiative internal conversion in the S_1 state is expected to be enhanced by this structural change. The observed fluorescence lifetime has been found to be much shorter than the calculated radiative lifetime, indicating that the fluorescence quantum yield is low. The lifetime of phenanthrene-d_{10} is longer than that of phenanthrene-h_{10} (normal deuterium effect). This fact is in contrast with anthracene, which is a structural isomer of phenanthrene. The lifetime at the S_1 zero-vibrational level of anthracene-d_{10} is much shorter than that of anthracene-h_{10} (inverse deuterium effect). In phenanthrene, the lifetime becomes monotonically shorter as the vibrational energy increases for both isotopical molecules without marked vibrational dependence. The vibrational structure of the S_0 state is considered to be homogeneous and quasi-continuous (statistical limit) in the S_1 energy region. © *2012 American Institute of Physics*. [http://dx.doi.org/10.1063/1.3703755]

I. INTRODUCTION

Phenanthrene is one of the prototypical molecules of nonlinear catacondensed aromatic hydrocarbons. Extensive spectroscopic studies have been carried out in both solid phase[1–10] and gas phase.[11–20] Theoretical calculations have also been performed.[21–23] It is of great interest and importance to investigate electronic, vibrational, and rotational structures of isolated molecules, that are closely related to the radiative and nonradiative transitions in the electronic excited state. The structure and excited-state dynamics have recently been clarified by high-resolution spectroscopy on benzene,[24–27] linear polyacene,[28–36] and pericondensed polycyclic aromatic hydrocarbons (PAHs).[37–39] These molecules are planar and possess high D_{2h} symmetry (D_{6h} for benzene) both in the ground electronic state (S_0) and the first excited singlet state (S_1), whereas the phenanthrene molecule is expected to possess C_{2v} symmetry by those previous studies.

Generally for PAH molecules, the second excited singlet state (S_2) is close in energy to the S_1 state. The energy of HOMO → LUMO excitation is expected to be the smallest in the possible electronic excitations. This configuration gives a strong absorption band in the ultraviolet region, which is designated as ^1L_a.[40] The next two configurations of HOMO → LUMO+1 and HOMO−1 → LUMO are nearly degenerate. These two excited states, therefore, strongly interact and the excitation energy of one of them is lowered so as to be comparable with the HOMO → LUMO configuration. The absorption is weak, and the band is designated as ^1L_b. The S_1 state of naphthalene is the latter ^1L_b ($^1B_{3u}$), in which the absorption is weak and the fluorescence lifetime is long (∼300 ns). In contrast, the S_1 state is ^1L_a ($^1B_{2u}$) for anthracene, which originates from the HOMO → LUMO configuration. The $S_1 \leftarrow S_0$ absorption is strong and the fluorescence lifetime is short (<30 ns). As for phenanthrene, the $S_1 \leftarrow S_0$ absorption has been found to be weak and is identified as ^1L_a.[20] It is important to observe and analyze the rotationally resolved spectrum to clarify the structure and properties of the S_0 and S_1 states.

The geometrical structure is strongly correlated with the radiationless transitions in the electronic excited state. In anthracene, which is a structural isomer of phenanthrene, it was demonstrated that the nonradiative relaxation was considerably enhanced by deuterium substitution at the zero-vibrational level of the S_1 state.[30–33] This is called the *inverse deuterium effect* because radiationless transitions are normally slower in deuterated compounds. The main nonradiative process is internal conversion (IC) to the S_0 state. This is caused by nonadiabatic vibronic interaction.[33] Intersystem crossing (ISC) to the triplet state is generally expected to be very slow in PAH molecules.[41,42] It is well known that the ISC yield is considerably high for naphthalene and anthracene in cold solid. The difference from gas molecules is attributed to intermolecular interaction. The ISC is efficiently induced by breaking of molecular planarity. The naphthalene and

a)Author to whom correspondence should be addressed. Electronic mail: baba@kuchem.kyoto-u.ac.jp.

anthracene molecules are planar in the gas phase and ISC is expected to be very slow by El-Sayed's rule.[41]

In this article, we present the experimental results of measurements of fluorescence excitation spectra, lifetimes for single vibronic level excitations of jet-cooled phenanthrene-h_{10} and phenanthrene-d_{10}, and the rotationally resolved ultrahigh-resolution spectrum of phenanthrene-h_{10}. We discuss the electronic, vibrational, and rotational structures of phenanthrene, and the mechanism of IC in the S_1 state on the basis of stable geometrical structures in the S_0 and S_1 states.

II. EXPERIMENTAL

Commercially obtained phenanthrene-h_{10} (Wako Chemical, 98%) and phenanthrene-d_{10} (CDN Isotopes, 98.4%) were used without further purification. The solid sample was heated to 120 °C in a stainless steel container and the vapor was mixed with Ar gas (1.2 atm). The mixed gas was expanded into a vacuum chamber through a pulsed nozzle (an automobile electric fuel injector) to generate a supersonic jet. As a light source, we employed a tunable dye laser (Lambda Physik LPD 3002, $\Delta E = 0.1$ cm^{-1}, DCM) pumped by a pulsed excimer laser (Coherent Compex Pro 110, 308 nm, 200 mJ). The ultraviolet light was obtained by second harmonic generation using a potassium dihydrogen phosphate (KDP) crystal. Fluorescence from excited molecules was collected using a lens and sent to a photomultiplier (Hamamatsu R928). The output was amplified using a preamplifier (Stanford Research SR240) and was processed by a box-car integrator (Stanford Research SR250). The change in fluorescence intensity with the laser light wavelength was recorded as a fluorescence excitation spectrum. The decay curve of fluorescence intensity was recorded using a storage oscilloscope (LeCroy 9362), and the lifetime value was determined by a least-squares fitting to the calculated curve taking account of the laser pulse duration and time response in the electric signal output.

A rotationally resolved ultrahigh-resolution spectrum was obtained using a CW single-mode ring dye laser (Coherent CR899-29, $\Delta E = 0.0001$ cm^{-1}, DCM) pumped by a Nd:YVO_4 laser (Spectra-Physics, Millennia X, 532 nm, 10 W). The ultraviolet light was generated using an enhancement cavity (Spectra-Physics, Wavetrain-SC, BBO). The power at 341 nm was 10 mW. The supersonic jet was collimated using a conical skimmer (2 mm orifice diameter) and was crossed with the laser light beam at right angles. Fluorescence from excited molecules was collected by a high reflection focusing system composed of an ellipsoidal mirror and a spherical mirror to a photomultiplier (Hamamatsu R585). The output was processed by a gated photoncounter (Stanford Research SR400). The observed spectral linewidth was 0.0006 cm^{-1}, which was mainly due to the residual Doppler width in our setup. In order to calibrate the transition wavenumber of each rotational line, we recorded the frequency marks of a stabilized etalon (Burleigh CFT-500, FSR = 150 MHz) and a Doppler-free saturation spectrum of I_2. The absolute wavenumber was determined using a high-resolution spectral atlas with accuracy of 0.0004 cm^{-1}.[43]

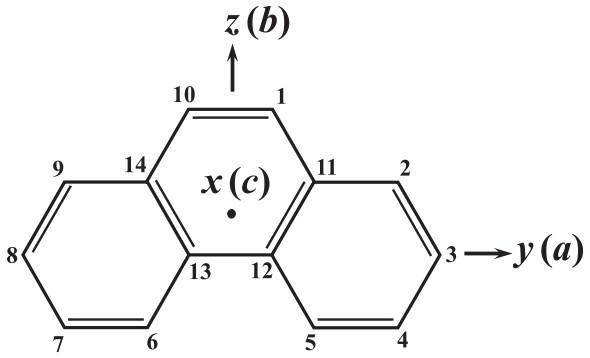

FIG. 1. Molecular structure, coordinate (rotational) axes, and numbering of carbon atoms in phenanthrene.

III. RESULTS AND DISCUSSION

Figure 1 depicts the molecular structure, coordinate (rotational) axes, and the numbering of carbon atoms for phenanthrene. The molecule is assumed to be planar and two-fold symmetric with respect to the in-plane short axis (z). The in-plane long axis is taken as the y axis which is the principal rotational axis of a near-prolate asymmetric top (a). The c axis is perpendicular to the molecular plane (x). The fluorescence excitation spectra of jet-cooled phenanthrene-h_{10} and phenanthrene-d_{10} are depicted in Fig. 2. The 0_0^0 band is strong and many vibronic bands are observed in the higher excess energy region. The spectral feature is almost the same as those previously reported.[19,20] The vibrational energies of observed bands are listed in Tables I and II.

In order to identify the S_1 state and to carry out a normal-mode analysis of observed vibronic bands, we observed the rotational envelopes for a number of vibronic bands. The results are depicted in Fig. 3. The $\pi\pi^*$ state is represented by A_1 or B_2 (in-plane irreducible representation in the C_{2v} point group). First, we consider the $^1A_1 - {}^1A_1$ transition, in which the transition moment is parallel to the two-fold axis (z). This axis is the rotational b axis of a near-prolate asymmetric top ($A \gg B > C$) and the selection rules for the electronic transition are $\Delta J = 0, \pm 1$, $\Delta K_a = \pm 1$, and $\Delta K_c = \pm 1$ (b type). There is no strong rotational line near the band origin and

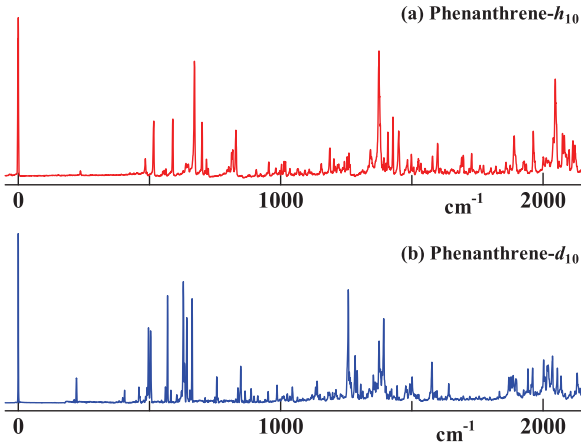

FIG. 2. Fluorescence excitation spectra of jet-cooled (a) phenanthrene-h_{10} and (b) phenanthrene-d_{10}.

TABLE I. Vibrational energies (cm^{-1}) and assignments of the bands observed in the fluorescence excitation spectrum of the $S_1\ ^1A_1 \leftarrow S_0\ ^1A_1$ transition of phenanthrene-h_{10}.

Band number	Vibrational energy	Band type	Assignment	Lifetime (ns)
1	0	*b*	0_0^0 (29324 cm^{-1})	76
2	154			75
3	238	*b*	23_0^1 (a_1)	
4	392	*b*	22_0^1 (a_1)	
5	425	*a*	66_0^1 (b_2)	67
6	442			71
7	484	*a*	65_0^1 (b_2)	75
8	516	*b*	21_0^1 (a_1)	77
9	559			73
10	565			71
11	589	*a*	64_0^1 (b_2)	74
12	651			73
13	668			74
14	672	*b*	20_0^1 (a_1)	74
15	701	*a*	63_0^1 (b_2)	71
16	713			67
17	725			71
18	819	*b*	19_0^1 (a_1)	70
19	829	*a*	62_0^1 (b_2)	65
20	954	*a*	61_0^1 (b_2)	70
21	999			70
22	1006			67
23	1013	*a*	60_0^1 (b_2)	
24	1019	*a*	59_0^1 (b_2)	75
25	1036	*b*	18_0^1 (a_1)	
26	1065	*b*	17_0^1 (a_1)	70
27	1155	*b*	15_0^1 (a_1)	67
28	1188	*a*	58_0^1 (b_2)	72
29	1221	*a*	57_0^1 (b_2)	67
30	1243	*b*	14_0^1 (b_2)	68
31	1251			63
32	1260	*b*	15_0^1 (a_1)	
33	1265	*a*	56_0^1 (b_2)	
34	1278			69
35	1342	*b*	12_0^1 (a_1)	66
36	1374	*b*	11_0^1 (a_1)	70
37	1405			66
38	1408		55_0^1 (b_2)	
39	1428		54_0^1 (b_2)	68
40	1449		10_0^1 (b_2)	67
41	1483		9_0^1 (b_2)	
42	1501			68
43	1524		52_0^1 (b_2)	67
44	1528			67
45	1534		8_0^1 (a_1)	
46	1578		7_0^1 (a_1)	67
47	1597		50_0^1 (b_2)	67
48	1700			64
49	1730			64
50	1892			63
51	1969			63
52	2050			63
53	2078			63
54	2208			63

TABLE II. Vibrational energies (cm^{-1}) and assignments of the bands observed in the fluorescence excitation spectrum of the $S_1\ ^1A_1 \leftarrow S_0\ ^1A_1$ transition of phenanthrene-d_{10}.

Band number	Vibrational energy	Band type	Assignment	Lifetime (ns)
1	0	*b*	0_0^0 (29419 cm^{-1})	113
2	222	*b*	23_0^1 (a_1)	113
3	385	*b*	22_0^1 (a_1)	
4	405	*a*	66_0^1 (b_2)	105
5	460	*a*	65_0^1 (b_2)	107
6	496			102
7	504	*b*	21_0^1 (a_2)	106
8	562			99
9	569	*a*	64_0^1 (b_2)	105
10	583			102
11	598			99
12	629			102
13	634			104
14	642	*b*	20_0^1 (a_1)	
15	655			98
16	662	*a*	63_0^1 (b_2)	103
17	749	*a*	62_0^1 (b_2)	
18	756	*b*	19_0^1 (a_1)	113
19	848			104
20	887	*b*	15_0^1 (a_1)	102
21	953	*a*	58_0^1 (b_2)	106
22	986	*b*	14_0^1 (a_1)	95
23	1006	*a*	57_0^1 (b_2)	
24	1045			110
25	1133		56_0^1 (b_2)	98
26	1139	*b*	13_0^1 (a_1)	96
27	1210	*b*	12_0^1 (a_1)	
28	1218			96
29	1284	*a*	55_0^1 (b_2)	96
30	1285			96
31	1305		11_0^1 (a_1)	
32	1330		54_0^1 (b_2)	
33	1375			92
34	1394			88
35	1401		10_0^1 (a_1)	
36	1409		53_0^1 (b_2)	88
37	1443		9_0^1 (a_1)	
38	1451		52_0^1 (b_2)	
39	1477		8_0^1 (a_1)	
40	1501			86
41	1526		7_0^1 (a_1)	
42	1547		51_0^1 (b_2)	90
43	1576		50_0^1 (b_2)	90
44	1580			90
45	1640		6_0^1 (a_1)	84
46	1871			81
47	1943			80
48	2003			78
49	2055			80
50	2130			81

two broad peaks of *P* and *R* branches are seen in the rotational envelope. In contrast, the transition moment of the $^1B_2 - {}^1A_1$ transition is parallel to the in-plane long axis (*y*). This is the *a* axis of an asymmetric top and the selection rules

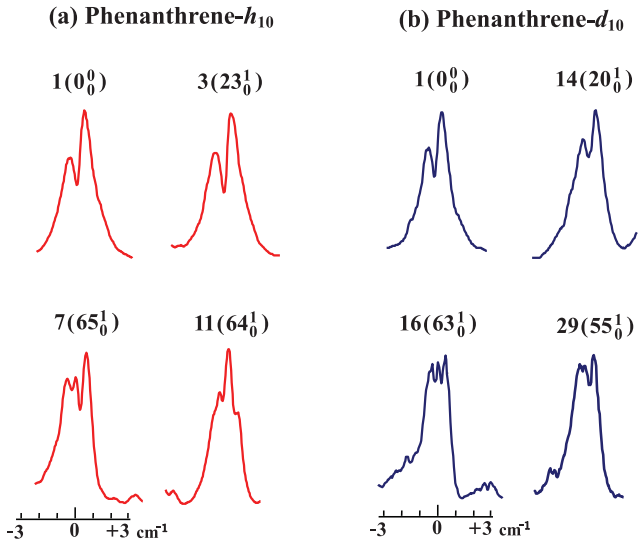

FIG. 3. Rotational envelopes of vibronic bands of (a) phenanthrene-h_{10} and (b) phenanthrene-d_{10}.

are $\Delta J = 0, \pm 1$, $\Delta K_a = 0$, and $\Delta K_c = \pm 1$ (a type). In this case, a sharp peak of the Q branch with $\Delta J = 0$, $\Delta K_a = 0$ transitions is observed near the band origin in addition to the P and R broad peaks. It is evident in Fig. 3 that the 0_0^0 band of phenanthrene-h_{10} is a b-type band and the S_1 state is identified to be $^1A_1$. One can see the a-type envelope for the $0_0^0 + 425$ cm^{-1} band, which is assigned to be a transition to a b_2 vibrational level in the S_1 $^1A_1$ state. Although this transition has zero Franck-Condon factor by symmetry, this vibronic band gains intensity through nonadiabatic vibronic interaction with the S_2 $^1B_2$ state (vibronic intensity borrowing). The transition to an a_1 vibrational level has nonzero Franck-Condon factor. It has been demonstrated, however, that the intensity mainly arises from vibronic interaction with the S_3 $^1A_1$ state.[20] The prominent vibronic bands are thus assigned to the transitions to a_1 and b_2 vibrational bands.

We performed *ab initio* theoretical calculations of vibrational energies with geometry optimization in the S_0 and S_1 states of phenanthrene-h_{10} and phenanthrene-d_{10} using the GAUSSIAN 09 program package.[44] All of the resultant values are listed in Table III. We first calculated the geometrical structure in the S_0 state by the MP2/6-311++G(d, p) method with geometry optimization, which provided the closest values of rotational constants to the experimentally obtained ones as described later. The vibrational energies were calculated by the DFT(CAM-B3LYP)/6-311++G(d, p) method with the respective optimized geometrical structure. We obtained the best value of scaling factor 0.982 by a least-squares fitting to the experimental values of phenanthrene-h_{10}, which were previously reported by Warren *et al.*[20]

For the S_1 $^1A_1$ state, we performed a similar procedure. The optimized structure was obtained by the CASSCF/cc-pVDZ method and the vibrational energies were calculated by the TD-DFT(CAM-B3LYP)/cc-pVDZ method. The best scaling factor was found to be 0.990 through the fit to the experimental values that were obtained from the fluorescence excitation spectrum in this work. The observed prominent vibronic bands in the fluorescence excitation spectra of phenanthrene-h_{10} and phenanthrene-d_{10} were unambiguously assigned by these procedures; the results are presented in Tables I and II, respectively.

It is noted that many vibronic bands are observed in the fluorescence excitation spectrum, suggesting that the stable molecular structure is markedly changed upon the $S_1 \leftarrow S_0$ electronic excitation. In order to confirm this structural change, we observed the rotationally resolved ultrahigh-resolution spectrum of the 0_0^0 band of phenanthrene-h_{10}; the result is depicted in Fig. 4(a). The phenanthrene molecule is a near-prolate asymmetric top. We analyzed the rotational level structure using the A-reduced Hamiltonian method presented by Watson.[45] The nonvanishing matrix elements are given by

$$\begin{aligned}\langle JKM|H_r^{(A)}|JKM\rangle &= \frac{1}{2}(B+C)J(J+1) + \left[A - \frac{1}{2}(B+C)\right]K^2 \\ &\quad - \Delta_J J^2(J+1)^2 - \Delta_{JK} J(J+1)K^2 - \Delta_K K^4, \quad (1)\end{aligned}$$

$$\begin{aligned}\langle JK \pm 2M|H_r^{(A)}|JKM\rangle &= \left\{\frac{1}{4}(B-C) - \delta_J J(J+1) - \frac{1}{2}\delta_K\left[(K\pm 2)^2 + K^2\right]\right\} \\ &\quad \times \{[J(J+1) - K(K\pm 1)] \\ &\quad \times [J(J+1) - (K\pm 1)(K\pm 2)]\}^{1/2}, \quad (2)\end{aligned}$$

where $|JKM\rangle$ is the eigenfunction of a symmetric top molecule. J is the quantum number of total angular momentum $\boldsymbol{J}$, while K and M are quantum numbers of the projection of $\boldsymbol{J}$ along the molecule-fixed $a(y)$ axis and the space-fixed Z axis, respectively. A, B, and C are the rigid-rotor rotational constants. Δ_J, Δ_{JK}, and Δ_K are the symmetric top quartic centrifugal distortion constants, and δ_J and δ_K are the asymmetric top distortion constants. The phenanthrene molecule possesses five pairs of identical hydrogen atoms in C_{2v} symmetry, and the statistical weights of nuclear spin are *ee*: *eo*: *oe*: *oo* = 33: 31: 33: 31.

First, we estimated the rigid rotor rotational constants by *ab initio* calculation with geometry optimization. A number of prominent rotational lines were assigned and we obtained the better constants by a least-squares fitting. We iteratively repeated this procedure and obtained the final values of rotational constants at the zero-vibrational levels in the S_0 and S_1 states. The resultant values are listed in Table IV. The calculated spectrum using these rotational constants (rotational temperature $T_{rot} = 12$ K, linewidth $\Gamma = 0.001$ cm^{-1}) is shown in Fig. 4(b). The expanded observed spectrum in the P-branch region is depicted in Fig. 5. The calculated spectrum shows good agreement with the observed spectrum, indicating that the obtained rotational constants are substantially accurate and reliable. The relative intensities, however, are remarkably different for several prominent lines. These are transitions for high J and K_a levels, and the discrepancy is considered to be attributed to large values of higher-order terms such as Δ_K and δ_K. The inertial defect $\Delta = I_c - I_b - I_a$ is very small and the assigned lines are all $\Delta K_a = \pm 1$, $\Delta K_c = \pm 1$ transition. The phenanthrene molecule is, therefore, essentially planar (C_{2v})

TABLE III. Calculated and observed vibrational energies (cm^{-1}) in the $S_0\ ^1A_1$ and $S_1\ ^1A_1$ states of phenanthrene-h_{10} and phenanthrene-d_{10}.

			$S_0\ ^1A_1$		$S_1\ ^1A_1$	
			h_{10}	d_{10}	h_{10}	d_{10}
Symmetry	Number	Vibration type	Calc.[a](Obs.)[b]	Calc.[c]	Calc.[a](Obs.)[b]	Calc.[c](Obs.)[d]
a_1	1	C-H stretch	3254	2406	3319	2453
	2	C-H stretch	3239	2396	3296	2441
	3	C-H stretch	3222	2385	3282	2430
	4	C-H stretch	3217	2374	3278	2424
	5	C-H stretch	3206	2364	3257	2404
	6	C-H bend + deform	1711	1688	1680	1659 (1640)
	7	C-H bend + deform	1612 (1613)	1574	1544 (1578)	1517 (1526)
	8	C-H bend + deform	1573 (1580)	1519	1510 (1534)	1480 (1477)
	9	C-H bend + deform	1523 (1526)	1484	1491 (1483)	1439 (1443)
	10	C-H bend + deform	1485 (1450)	1447	1439 (1449)	1389 (1401)
	11	C-H bend + deform	1430 (1423)	1346	1371 (1374)	1247 (1305)
	12	C-H bend + deform	1388 (1355)	1248	1305 (1342)	1198 (1210)
	13	C-H bend + deform	1297	1172	1236 (1260)	1031 (1139)
	14	C-H bend + deform	1272 (1257)	1015	1217 (1243)	1000 (986)
	15	C-H bend + deform	1186 (1199)	912	1138 (1155)	882 (887)
	16	C-H bend + deform	1171 (1165)	879	1116	853
	17	C-H bend + deform	1115	858	1067 (1065)	829
	18	C-H bend + deform	1067 (1063)	856	1057 (1036)	819
	19	ring deform	838 (833)	782	813 (819)	750 (756)
	20	ring deform	699 (714)	656	688 (672)	644 (642)
	21	ring deform	534 (544)	517	520 (516)	503 (504)
	22	ring deform	407 (408)	391	395 (392)	380 (385)
	23	skeletal deform	244 (246)	228	231 (238)	216 (222)
a_2	24	C-H bend + deform	955	823	942	852
	25	C-H bend + deform	936	781	904	776
	26	C-H bend + deform	908	748	846	748
	27	ring deform	830	725	802	691
	28	ring deform	746	617	709	578
	29	ring deform	721	574	684	559
	30	ring deform	524	451	519	435
	31	ring deform	488	335	482	402
	32	skeletal deform	379	420	367	320
	33	skeletal deform	218	201	224	203
	34	deform	74	67	92	84
b_1	35	C-H bend + deform	953	801	917	801
	36	C-H bend + deform	923	761	884	750
	37	C-H bend + deform	844	705	839	708
	38	ring deform	793	623	751	605
	39	ring deform	720	594	672	547
	40	ring deform	681	546	635	496
	41	ring deform	475	418	465	396
	42	ring deform	393	345	386	328
	43	skeletal deform	211	193	205	186
	44	butterfly	96	89		
b_2	45	C-H stretch	3242	2401	3299	2442
	46	C-H stretch	3235	2392	3284	2433
	47	C-H stretch	3216	2373	3276	2417
	48	C-H stretch	3208	2367	3257	2411
	49	C-H stretch	3204	2362	3252	2399
	50	C-H bend + deform	1647	1619	1645 (1597)	1621 (1576)
	51	C-H bend + deform	1616	1582	1596	1571 (1547)
	52	C-H bend + deform	1566	1498	1493 (1524)	1450 (1451)
	53	C-H bend + deform	1497	1445	1460	1398 (1409)
	54	C-H bend + deform	1463	1364	1403 (1428)	1343 (1330)
	55	C-H bend + deform	1434 (1434)	1310	1384 (1408)	1306 (1284)
	56	C-H bend + deform	1305	1067	1266 (1265)	1138 (1133)
	57	C-H bend + deform	1261	1031	1191 (1221)	975 (1006)

TABLE III. *(Continued.)*

Symmetry	Number	Vibration type	$S_0\ ^1A_1$ h_{10} Calc.[a](Obs.)[b]	$S_0\ ^1A_1$ d_{10} Calc.[c]	$S_1\ ^1A_1$ h_{10} Calc.[a](Obs.)[b]	$S_1\ ^1A_1$ d_{10} Calc.[c](Obs.)[d]
	58	C-H bend + deform	1197	967	1154 (1188)	949 (953)
	59	C-H bend + deform	1161	876	1110 (1019)	836
	60	C-H bend + deform	1057 (1019)	862	1008 (1013)	813
	61	C-H bend + deform	998	851	965 (954)	798
	62	ring deform	865 (875)	779	853 (829)	758 (749)
	63	ring deform	723 (731)	682	706 (701)	663 (662)
	64	ring deform	612 (620)	590	600 (589)	577 (569)
	65	ring deform	501 (500)	475	486 (484)	461 (460)
	66	skeletal deform	445 (471)	415	435 (425)	404 (405)

[a]Results of DFT(CAM-B3LYP)/6-311++G(d, p) are scaled by 0.983.
[b]Determined by the dispersed fluorescence spectrum [Ref. 20].
[c]Results of TD-DFT(CAM-B3LYP)/cc-pVDZ are scaled by 0.990.
[d]Determined by the fluorescence excitation spectrum in this work.

and the S_1 state is identified to be $^1A_1$. The A, B, and C values in the S_1 state are about 1% larger than those in the S_0 state. In order to determine the structural parameters such as bond lengths and bond angles in the S_1 state, we tried several calculational methods with geometry optimization. The best values of rotational constants are listed in Table V(a). The experimentally obtained rotational constants could be well reproduced by the MP2/6-311++G(d, p) calculation within the error of 0.02%. The obtained molecular structure is, therefore, considered to be the approximately true stable structure. The difference between the calculated and experimentally obtained rotational constants is less than 0.00001 cm^{-1}, which corresponds to the error of 2 mÅ in the C−C bond length. The calculated C−C bond lengths are listed in Table VI. This is assumed to be the limit in accuracy for the determination of stable geometrical structure.[27]

We performed similar calculations for the $S_1\ ^1A_1$ state. The best results were obtained by the CASSCF/cc-pVDZ calculation. The resultant rotational constants and C−C bond lengths are listed in Tables V(b) and VI, respectively. It should be noted that the C(2)−C(3), C(4)−C(5), and C(11)−C(12) bond lengths are markedly increased by the $S_1 \leftarrow S_0$ excitation. This structural change can be understood by the π molecular orbitals, which are illustrated in Fig. 6. The S_1 state is expressed as a linear combination of two configurations, ϕ_{47}(HOMO) → ϕ_{49}(LUMO+1) and ϕ_{46}(HOMO−1) → ϕ_{48}(LUMO). In particular, the C(11)−C(12) π bond is anti-bonding in ϕ_{48} and ϕ_{49}, leading to the smaller bond order and larger bond length.

When the structures and potential curves differ between the S_0 and S_1 states, it is assumed that the IC nonradiative process is fast and that the fluorescence quantum yield is low in the S_1 state. We observed the fluorescence decay curve and determined the lifetimes for single vibronic levels, which are plotted against the excess vibrational energy

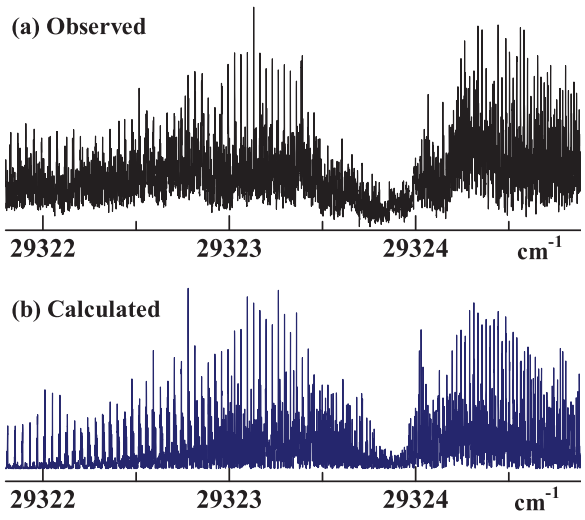

FIG. 4. (a) Observed rotationally resolved fluorescence excitation spectrum of the 0_0^0 band of phenanthrene-h_{10} and (b) calculated one using the obtained rotational constants.

TABLE IV. Molecular constants of the $S_0\ ^1A_1(v'' = 0)$, and $S_1\ ^1A_1(v' = 0)$ states of phenanthrene-h_{10}. Rotational constants, band origin T_0, and standard deviation σ are in units of cm^{-1}. Moments of inertia I_a, I_b, I_c and inertial defect Δ are in units of kg m^2.

Phenanthrene-h_{10}	$S_0\ ^1A_1(v'' = 0)$	$S_1\ ^1A_1(v' = 0)$
A	0.053594(14)	0.053266(12)
B	0.0183351(29)	0.0181409(28)
C	0.0136612(18)	0.0135258(17)
$\Delta_K(\times 10^{-7})$	–1.57(58)	–2.34(54)
$\Delta_{JK}(\times 10^{-8})$	3.4(17)	9.0(16)
$\Delta_J(\times 10^{-8})$	1.05(12)	1.00(11)
$\delta_K(\times 10^{-7})$	2.56(15)	2.31(15)
$\delta_J(\times 10^{-9})$	5.06(59)	4.98(54)
κ	–0.7658	–0.7678
$I_a(\times 10^{-46})$	52.231	52.553
$I_b(\times 10^{-46})$	152.67	154.31
$I_c(\times 10^{-46})$	204.91	206.96
$\Delta(\times 10^{-46})$	0.00282	0.09804
T_0	...	27323.877(3)
σ	...	0.0022
fit lines	...	726
band type		b

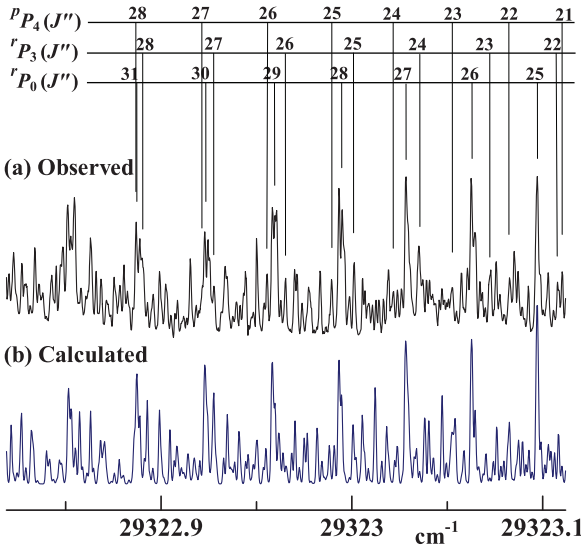

FIG. 5. (a) Expanded observed spectrum for the P branch region of the 0_0^0 band of phenanthrene-h_{10} and (b) calculated one using the obtained rotational constants. The assignments are shown above the spectrum. The superscript and subscript indicate ΔK_a and K'', respectively.

of the S_1 state in Fig. 7. The lifetime becomes shorter as the excess vibrational energy increases without any mode-selectivity for the vibrational levels. Although the fluorescence quantum yields were reported to be 0.13 and 0.11 for phenanthrene-h_{10} and phenanthrene-d_{10}, respectively, in EPA glass at 77 K,[5] it is difficult to experimentally determine them for the isolated molecule, because the $S_1 \leftrightarrow S_0$ transition is very weak. We, therefore, estimated it by the TD-DFT(CAM-B3LYP)/cc-pVDZ calculation of oscillator strength and obtained $f = 0.001$. The calculated f value considerably depended on the basis set. The accuracy is estimated to be $\pm$ 50%. The radiative lifetime is given by[46]

$$\tau_r = 1.500 \frac{1}{\nu^2 f} = 1740 \text{ ns}, \tag{3}$$

where ν is the transition wavenumber in units of cm^{-1}. The fluorescence quantum yield is represented by

$$\phi_F = \frac{1/\tau_r}{1/\tau_{nr} + 1/\tau_r}, \tag{4}$$

TABLE V. Experimentally obtained rigid rotational constants and the closest calculated ones (cm^{-1}) for the S_0 $^1A_1$ and S_1 $^1A_1$ states of phenanthrene-h_{10}.

	A	B	C
(a) S_0 $^1A_1$			
Exp. ($v'' = 0$)	0.053594	0.0183351	0.0136612
MP2/6-311++G(d, p)	0.0535866	0.0183353	0.0136610
(b) S_1 $^1A_1$			
Exp. ($v' = 0$)	0.053266	0.0181409	0.0135258
CASSCF/cc-pVDZ	0.0532242	0.0181362	0.0135269

TABLE VI. Calculated C–C bond lengths (Å) in the S_0 $^1A_1$ and S_1 $^1A_1$ states of phenanthrene.

	S_0 $^1A_1$[a]	S_1 $^1A_1$[b]
$R_{C\text{-}C}$(10-1)	1.3668	1.3799
$R_{C\text{-}C}$(1-11)	1.4331	1.4126
$R_{C\text{-}C}$(11-2)	1.4158	1.4312
$R_{C\text{-}C}$(2-3)	1.3848	1.4318
$R_{C\text{-}C}$(3-4)	1.4093	1.4197
$R_{C\text{-}C}$(4-5)	1.3872	1.4263
$R_{C\text{-}C}$(5-12)	1.4160	1.4369
$R_{C\text{-}C}$(11-12)	1.4272	1.4794
$R_{C\text{-}C}$(12-13)	1.4526	1.4554

[a]Results of MP2/6-311++G(d, p).
[b]Results of CASSCF/cc-pVDZ.

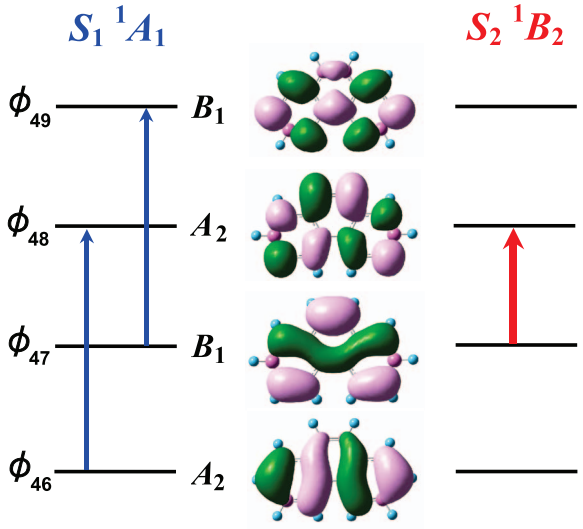

FIG. 6. π molecular orbitals of phenanthrene.

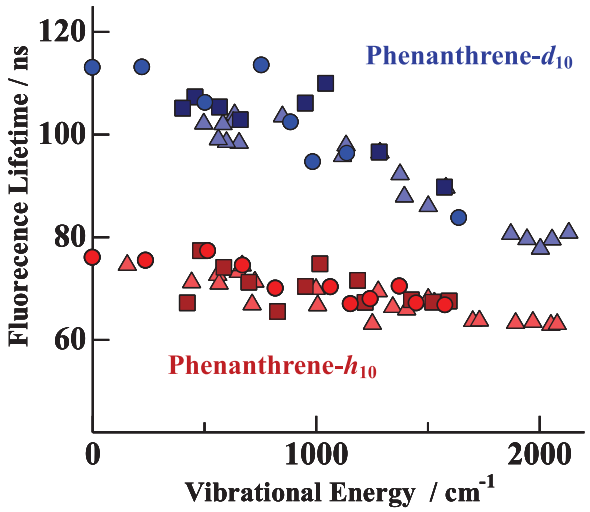

FIG. 7. Fluorescence lifetimes are plotted against the vibrational energies. The a_1, b_2, and unassigned levels are represented by circles, squares, and triangles, respectively.

where τ_{nr} is the nonradiative lifetime. The observed fluorescence lifetimes

$$\tau_F = \frac{1}{1/\tau_{nr} + 1/\tau_r} \tag{5}$$

are 76 and 113 ns. Finally, we obtained $\phi_F = 0.05$ and 0.07 for phenanthrene-h_{10} and phenanthrene-d_{10}, respectively. This indicates that the nonradiative transition dominates the relaxation process in the S_1 state of phenanthrene.

For planar PAH molecules in the gas phase, it has been demonstrated that the main nonradiative process in the S_1 state is not ISC to the triplet state, but IC to the S_0 state.[28,29,33,42] The IC rate at the zero-vibrational level in the S_1 state is given by[47–50]

$$\begin{aligned} W_{IC} &= \frac{2\pi}{\hbar} \sum_i \left| \langle \phi_{S_0} | \frac{\partial}{\partial Q_i} | \phi_{S_1} \rangle \right|^2 \left| \left\langle \chi_{S_0}^{v''} \middle| \frac{\partial}{\partial Q_i} \middle| \chi_{S_1}^{v'=0} \right\rangle \right|^2 \\ &\quad \times \delta\left(E_{S_1}^{v'=0} - E_{S_0}^{v''}\right) \\ &\simeq \frac{2\pi}{\hbar} \frac{\sum_i \left| \langle \phi_{S_0}(r, Q_0) | \left(\frac{\partial U(r,Q)}{\partial Q_i} \right)_{Q_0} | \phi_{S_1}(r, Q_0) \rangle \right|^2}{\{E_{S_1}(Q_0) - E_{S_0}(Q_0)\}^2} \\ &\quad \times \left| \left\langle \chi_{S_0}^{v''}(Q_i) \middle| \frac{\partial}{\partial Q_i} \middle| \chi_{S_1}^{v'=0}(Q_i) \right\rangle \right. \\ &\quad \left. \times \prod_{j \neq i} \left\langle \chi_{S_0}^{v''}(Q_j) \middle| \chi_{S_1}^{v'=0}(Q_j) \right\rangle \right|^2 \\ &\quad \times \delta\left(E_{S_1}^{v'=0} - E_{S_0}^{v''}\right), \end{aligned} \tag{6}$$

where ϕ_{S_0} and ϕ_{S_1} are the electronic wavefunctions of the S_0 and S_1 states, respectively, $\chi_{S_0}^{v''}$ the vibrational wavefunction of the high-vibrational level in the S_0 state, and $\chi_{S_1}^{v'=0}$ that of the zero-vibrational level in the S_1 state. δ is the Dirac delta function, and Q_i is a normal coordinate. The second and third matrix elements are the nonadiabatic Franck-Condon overlap of a promoting mode and the Franck-Condon overlap of other modes, respectively. In C_{2v} symmetry, the S_1 $^1A_1$ state couples with the S_0 $^1A_1$ state through an a_1 vibration. If the potential energy curves in the S_1 state are similar to those in the S_0 state, the nonadiabatic Franck-Condon factor becomes smaller as the $S_1 - S_0$ excitation energy increases (energy gap law).[47] There are two cases that give rise to the large IC rate. One is *displacement*, in which the stable geometrical structures at the potential minima are considerably different (different rotational constants). Another is *distortion*, in which the curvature of potential energy curves are different (different vibrational energies). As shown in Table III, the observed vibrational energies of a_1 modes in the S_1 state are very similar to those in the S_0 state, indicating that the distortion is not the main cause of the large IC rate in phenanthrene. The geometrical structure in the S_1 state, however, is remarkably different from that in the S_0 state, although the change in rotational constants are not very large in this case. It is considered that IC is enhanced by the displacement for the C(11)−C(12) bond length in particular.

The IC rate is proportional to the nonadiabatic Franck-Condon overlap, which is expected to depend on the vibrational mode in the S_1 state. In fact, the fluorescence lifetime has been demonstrated to change with the vibrational level in the S_1 state for a number of PAH molecules.[29,33,38] For phenanthrene, it has been found to be almost independent of the vibrational level, indicating that the vibrational structure is quasi-continuous and homogeneous (statistical limit) in the energy region of fundamental vibrational levels of the S_1 state. In contrast, the IC rate is markedly dependent on the vibrational level in anthracene, which is a structural isomer of phenanthrene with the same molecular size.[31] The coupling level density of the S_0 state is considered to be much higher in phenanthrene because of its lower symmetry and larger $S_1 \leftarrow S_0$ excitation energy.

Radiationless transitions are normally depressed by deuterium substitution, which reduces the zero-point energy and increases the number of quanta in the accepting modes. Actually, the fluorescence lifetime of phenanthrene-d_{10} is remarkably longer than that of phenanthrene-h_{10}. It should be noted that the fluorescence lifetime at the zero-vibrational level in the S_1 state of anthracene-d_{10} is much shorter than that of anthracene-h_{10}.[30–33] Further studies are needed to clarify the mechanism of the inverse deuterium effect, because we were unable to obtain any useful information in this regard from the deuterium effect in phenanthrene.

IV. SUMMARY

We observed fluorescence excitation spectra of the S_1 $^1A_1 \leftarrow S_0$ $^1A_1$ transition of jet-cooled phenanthrene-h_{10} and phenanthrene-d_{10}. The observed vibronic bands were assigned by referring to the results of *ab initio* theoretical calculations. The rotational constants were determined for the zero-vibrational levels in the S_0 and S_1 states of phenanthrene-h_{10} via the ultrahigh-resolution fluorescence excitation spectrum. The MP2/6-311++G(d, p) and CASSCF/cc-pVDZ calculations with geometry optimization revealed that the values of the rotational constants were close to the experimentally obtained ones for the S_0 and S_1 states, respectively. It has been demonstrated that the molecule is planar (C_{2v}) and that the stable geometrical structure is markedly changed upon the $S_1 \rightarrow S_0$ electronic excitation. This structural change is considered to be the main cause of fast IC in the S_1 state of phenanthrene. The IC rate of phenanthrene-d_{10} is smaller than that of phenanthrene-h_{10}, which is in accordance with the general rule that radiationless transition is depressed by deuterium substitution.

ACKNOWLEDGMENTS

This research was supported by a grant-in-aid for the Global COE Program, "International Center for Integrated Research and Advanced Education in Materials Science," from the Ministry of Education, Culture, Sports, Science, and Technology of Japan. The experiment was supported by the Inter-University Network for Efficient Utilization of

Chemical Research Equipments. M. Baba would like to thank Dr. S. Kasahara (Kobe University) for his kind help.

[1]D. S. McClure, J. Chem. Phys. **25**, 481 (1956).
[2]T. Azumi and S. P. McGlynn, J. Chem. Phys. **37**, 2413 (1962).
[3]R. M. Hochstrasser and G. J. Small, J. Chem. Phys. **45**, 2270 (1966).
[4]J. B. Gallivan and J. S. Brinen, J. Chem. Phys. **30**, 1590 (1969).
[5]R. Li and E. C. Lim, J. Chem. Phys. **57**, 605 (1972).
[6]M. A. El-Sayed, W. R. Moomaw, and J. B. Chodak, Chem. Phys. Lett. **20**, 11 (1973).
[7]V. Schettino, N. Neto, and S. Califano, J. Chem. Phys. **44**, 2724 (1966).
[8]V. Schettino, J. Chem. Phys. **46**, 302 (1967).
[9]A. Bree, F. G. Solven, and V. V. B. Vilkos, J. Mol. Spectrosc. **44**, 298 (1972).
[10]A. I. Alajtal, H. G. M. Edwards, M. A. Elbagerma, and I. J. Scowen, Spectrochim. Acta, Part A **76**, 1 (2010).
[11]D. P. Craig and R. D. Gordon, Proc. R. Soc. London, Ser. A **288**, 69 (1965).
[12]D. P. Craig and G. J. Small, J. Chem. Phys. **50**, 3827 (1969).
[13]J. A. Piest, J. Oomems, J. Bakker, G. von Helden, and G. Meijer, Spectrochim. Acta, Part A **57**, 717 (2001).
[14]E. Cané, A. Miani, P. Palmieri, R. Tarroni, and A. Trombetti, Spectrochim. Acta, Part A **53**, 1839 (1997).
[15]A. J. Huneycutt, R. N. Casaes, B. J. McCall, C. Y. Chung, Y. P. Lee, and R. J. Saykally, ChemPhysChem. **5**, 321 (2004).
[16]D. J. Cook, S. Schlemmer, N. Balucani, D. R. Wagner, J. A. Harrison, B. Steiner, and R. J. Saykally, J. Phys. Chem. A **102**, 1465 (1998).
[17]J. Clairemidi, P. Bréchignac, G. Moreels, and D. Pautet, Planet. Space Sci. **52**, 761 (2004).
[18]A. Amirav, M. Sonnenschein, and J. Jortner, J. Phys. Chem. **88**, 5593 (1984).
[19]N. Ohta and H. Baba, Mol. Phys. **59**, 921 (1986).
[20]J. A. Warren, J. M. Hayes, and G. J. Small, Chem. Phys. **102**, 323 (1986).
[21]R. Firouzi and M. Zahedi, J. Mol. Struct.: THEOCHEM **862**, 7 (2008).
[22]S. R. Langhoff, J. Phys. Chem. **100**, 2819 (1996).
[23]J. M. L. Martin, J. El-Yazal, and J.-P. Francois, J. Phys. Chem. **100**, 15358 (1996).
[24]A. Doi, S. Kasahara, H. Katô, and M. Baba, J. Chem. Phys. **120**, 6439 (2004).
[25]A. Doi, M. Baba, S. Kasahara, and H. Katô, J. Mol. Spectrosc. **227**, 180 (2004).
[26]M. Okruss, R. Müller, and A. Hese, J. Mol. Spectrosc. **193**, 293 (1999).
[27]M. Baba, Y. Kowaka, T. Ishimoto, U. Nagashima, H. Goto, and N. Nakayama, J. Chem. Phys. **135**, 054305 (2011).
[28]M. Okubo, J. Wang, M. Baba, and H. Katô, J. Chem. Phys. **116**, 9293 (2002).
[29]K. Yoshida, Y. Semba, S. Kasahara, T. Yamanaka, and M. Baba, J. Chem. Phys. **130**, 194304 (2009).
[30]S. Okajima, B. E. Forch, and E. C. Lim, J. Phys. Chem. **87**, 4571 (1983).
[31]W. R. Lambert, P. M. Felker, and A. H. Zewail, J. Chem. Phys. **81**, 2209 (1984).
[32]M. Sonnnenschein, A. Amirav, and J. Jortner, J. Phys. Chem. **88**, 4214 (1984).
[33]M. Baba, M. Saitoh, K. Taguma, K. Shinohara, K. Yoshida, Y. Semba, S. Kasahara, N. Nakayama, H. Goto, T. Ishimoto, and U. Nagashima, J. Chem. Phys. **130**, 134315 (2009).
[34]W. M. van Herpen, W. Leo Meerts, and A. Dynamus, J. Chem. Phys. **87**, 182 (1987).
[35]E. Heinecke, D. Hartmann, R. Müller, and A. Hese, J. Chem. Phys. **109**, 906 (1998).
[36]E. Heinecke, D. Hartmann, and A. Hese, J. Chem. Phys. **118**, 113 (2003).
[37]M. Baba, M. Saitoh, Y. Kowaka, K. Taguma, K. Yoshida, Y. Semba, S. Kasahara, Y. Ohshima, T. Yamanaka, Y.-C. Hsu, and S. H. Lin, J. Chem. Phys. **131**, 224318 (2009).
[38]Y. Kowaka, Y. Suganuma, N. Ashizawa, N. Nakayama, H. Goto, T. Ishimoto, U. Nagashima, and M. Baba, J. Mol. Spectrosc. **260**, 72 (2010).
[39]Y. Suganuma, Y. Kowaka, N. Ashizawa, N. Nakayama, H. Goto, T. Ishimoto, U. Nagashima, T. Ueda, T. Yamanaka, N. Nishi, and M. Baba, Mol. Phys. **109**, 1831 (2011).
[40]J. R. Platt, J. Chem. Phys. **17**, 484 (1949).
[41]M. A. El-Sayed, J. Chem. Phys. **38**, 2834 (1963).
[42]M. Baba, J. Phys. Chem. A **115**, 9514 (2011).
[43]B. Bodermann, H. Knöckel, and E. Tiemann, *IodineSpec4* (Toptica Photonics, 2002).
[44]M. J. Frisch, G. W. Trucks, H. B. Schlegel *et al.*, GAUSSIAN 09, Revision A.02, Gaussian, Inc., Wallingford, CT, 2009.
[45]J. K. G. Watson, in *Vibrational Spectra and Structure*, edited by J. R. Durig (Marcel Dekker, New York, 1977), Vol. 6, Chap. 1.
[46]R. A. Becker, *Theory and Interpretation of Fluorescence and Phosphorescence* (Wiley, New York, 1969).
[47]W. Siebrand, J. Chem. Phys. **46**, 440 (1967).
[48]S. H. Lin, J. Chem. Phys. **44**, 3759 (1966).
[49]C. H. Chin, H. Y.-J. Shin, H.-W. Wang, Y.-L. Chen, C.-C. Wang, S. H. Lin, and M. Hayashi, J. Chin. Chem. Soc. (Taipei) **53**, 131 (2006).
[50]M. Bixon and J. Jortner, J. Chem. Phys. **48**, 715 (1968).